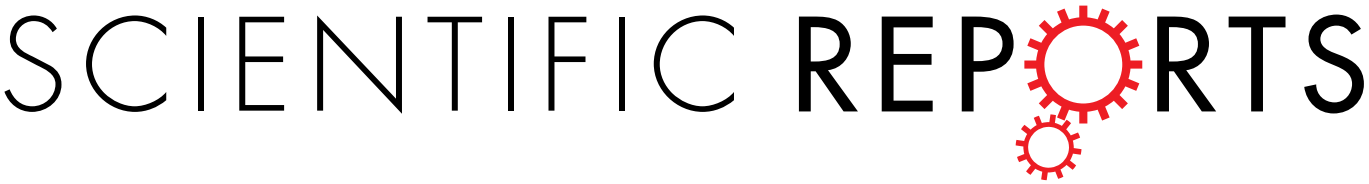

OPEN

# Simultaneous Electrochemical Deposition of Cobalt Complex and Poly(pyrrole) Thin Films for Supercapacitor Electrodes

Received: 27 November 2018
Accepted: 11 March 2019
Published online: 04 April 2019

Charlette M. Parnell[1], Bijay P. Chhetri[1], Travis B. Mitchell[1], Fumiya Watanabe[2], Ganesh Kannarpady[2], Ambar B. RanguMagar[1], Huajun Zhou[3], Karrer M. Alghazali[2], Alexandru S. Biris[2] & Anindya Ghosh[1]

**Supercapacitors are beneficial as energy storage devices and can obtain high capacitance values greater than conventional capacitors and high power densities compared to batteries. However, in order to improve upon the overall cost, energy density, and charge-discharge rates, the electrode material of supercapacitors needs to be fine-tuned with an inexpensive, high conducting source. We prepared a Co(III) complex and polypyrrole (PPy) composite thin films ($CoN_4$-PPy) that was electrochemically deposited on the surface of a glassy carbon working electrode. Cyclic voltammetry studies indicate the superior performance of $CoN_4$-PPy in charge storage in acidic electrolyte compared to alkaline and organic solutions. The $CoN_4$-PPy material generated the highest amount of specific capacitance (up to 721.9 F/g) followed by Co salt and PPy (Co-PPy) material and PPy alone. Cyclic performance studies showed the excellent electrochemical stability of the $CoN_4$-PPy film in the acidic medium. Simply electrochemically depositing an inexpensive Co(III) complex with a high electrically conducting polymer of PPy delivered a superior electrode material for supercapacitor applications. Therefore, the results indicate that novel thin films derived from Co(III) metal complex and PPy can store a large amount of energy and maintain high stability over many cycles, revealing its excellent potential in supercapacitor devices.**

The widespread global energy consumption is slowly depleting our limited resources. With most of the energy production manufactured from non-renewable resources such as fossil fuels, it is essential to investigate alternative energy sources that are clean, efficient and renewable[1]. There are several types of renewable energy sources such as solar and wind energy that have been beneficial in providing energy to meet our needs[2,3]. However, to sufficiently provide energy during times of no sunlight or wind, a device that harvests and stores the energy needs to be implemented. Some examples of such devices that have been employed in this regard include batteries, capacitors and supercapacitors[4–6]. Compared to batteries, supercapacitors can deliver charge quickly for higher power density[7]. There are two types of supercapacitors: electrochemical double layer capacitors (EDLCs) and pseudocapacitors. The former non-Faradaically stores charge with an electrochemical double-layer while the latter uses Faradaic redox processes, electrosorption and/or intercalation processes[8]. The efficiency of supercapacitors lies within the electrode material as this can dramatically influence the surface area, conductivity and overall resistance of the device. Moreover, the cost of electrode materials hinders the widespread use of these devices[9]. Therefore, it is important to develop electrode materials that couple high capacitance (to improve charge-discharge cycling) with reduced material cost[10]. Liu *et al.* developed hollow, spherical nitrogen-rich porous carbon shells *via* carbonization of porous organic frameworks (POFs) to be used as an electrode material in a supercapacitor[11]. High capacitance up to 230 F/g was achieved at current density of 0.5 A/g with excellent cycling performance up to 1500 cycles. While designing POF electrodes in supercapacitor devices can give better

[1]Department of Chemistry, University of Arkansas at Little Rock, 2801 South University Avenue, Little Rock, AR, 72204, USA. [2]Center for Integrative Nanotechnology Sciences, University of Arkansas at Little Rock, 2801 South University Avenue, Little Rock, AR, 72204, USA. [3]High-Density Electronics Center, University of Arkansas, Fayetteville, AR, 72701, USA. Charlette M. Parnell and Bijay P. Chhetri contributed equally. Correspondence and requests for materials should be addressed to A.S.B. (email: asbiris@ualr.edu) or A.G. (email: axghosh@ualr.edu)

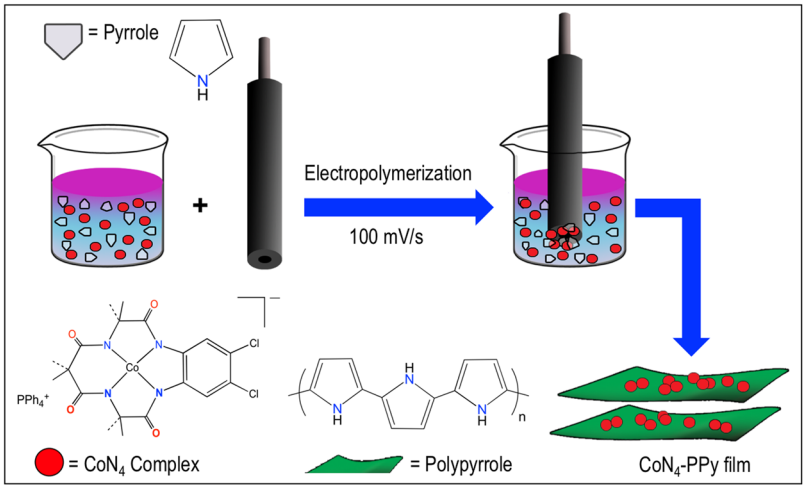


**Figure 1.** Schematic representation of electrochemical deposition of PPy films using pyrrole and $CoN_4$ complex. The films were deposited on GCE.

electrochemical stability in these materials, the capacitance still needs to be improved to meet the standards of commercialization of these devices.

Deviating from porous controllability, use of transition metal oxides such as $NiCo_2O_4$[12], $MoO_3$[13], and $MnO_2$[14] have been investigated as pseudocapacitive materials for supercapacitors owing to their low cost, different oxidation states, low toxicity, high power output, and high capacitance[15,16]. As for example, Lei *et al*. synthesized $NiCo_2O_4$ by rapid and template-free microwave-assisted heating reflux method to fabricate electrode materials for supercapacitors. These flower-shaped microspheres possess large specific surface area, which assisted in its high specific capacitance of 1006 F/g. Even after 1000 electrochemical cycles, the material retained 93.2% of its activity at current density of 8 A/g[12]. In the search of new class of electrode materials for supercapacitors, transition metal sulfides have also been investigated[16,17]. Shen *et al*. reported synthesis of $NiCo_2S_4$ nanosheets grown on nitrogen-doped carbon foams ($NiCo_2S_4$/NCF), which exhibited a ultrahigh capacitance of 1025 F/g at 10 A/g with excellent electrochemical cycling stability with only 9.6% loss of performance after 2000 cycles at 10 A/g[17]. Thus, a new approach incorporating inexpensive metals has shown to possess promising potential for electrochemical supercapacitors. Incorporating this idea and renewable materials, the performance and cost of supercapacitors and their electrode materials can be further improved.

Aside from investigating inexpensive metals, conducting polymers such as polyaniline (PANI)[18], polythiophene (PTh)[19], and polypyrrole (PPy)[20] have gained much attention throughout the scientific community as materials that can enhance capacitance efficiency for charge storage[21,22]. Among different conducting polymers, PPy has shown to be the most promising due to its high conductivity, low cost, and ease of synthesis. Moreover, PPy exhibits excellent redox reversibility and environmental stability[23]. There are two methods of PPy synthesis: chemical and electrochemical. Of the two synthetic routes, electrochemical deposition provides samples that are more conductive and exhibit a higher capacitance than those developed from chemical methods[24]. While several metal oxides and metal sulfides have been used to design electrode materials for fuel cells and supercapacitors, the use of metal complexes has been relatively low. Over the past few decades, extensive efforts have been made to design catalytic materials bearing macrocyclic metal $N_4$ complexes such as porphyrin and phthalocyanines[25,26]. The macrocyclic metal $N_4$ complexes with different transition metals have been identified as a promising electrode material for fuel cells[27–29] and lithium-air ($Li_2O_2$) battery[30]. Recently, we demonstrated the use of macrocyclic Co(III)[31] and Mn(III) $N_4$ complexes coated with polydopamine[32] and supported on graphene as a promising electrocatalyst for oxygen reduction reaction (ORR). In the past, research on metal $N_4$ complexes has mainly focused on the electrochemical ORR and covered less on supercapacitors. Thus, we extended our work on Co(III) $N_4$ macrocyclic complex for supercapacitors.

In this manuscript, we report the electrochemical deposition of PPy films onto a glassy carbon electrode (GCE). To increase the capacitance, Co metal impurities in the forms of either Co-amidomacrocyclic metal catalyst ($CoN_4$) or Co acetate salt, were integrated into the film network (Fig. 1). Of these impurities used, $CoN_4$ facilitated greater supercapacitive activity with a high specific capacitance up to 721.9 F/g. Galvanostatic charge-discharge (GCD) cycles were performed and revealed high rate of charge-discharge for $CoN_4$-PPy films. Furthermore, $CoN_4$-PPy films provided excellent electrochemical stability in acidic media as revealed by cyclic performance studies. Therefore, the use of Co(III) complex greatly enhanced the specific capacitance of PPy films. To the best of our knowledge, we are the first to develop a conductive electrode film using macrocyclic Co(III) $N_4$ complexes and conductive polymer (PPy) by electrodeposition which demonstrates superior supercapacitor performance. Our $CoN_4$-PPy film offers an exceptional platform for generating novel and inexpensive electrode materials and could be a significant improvement in the field of supercapacitors.

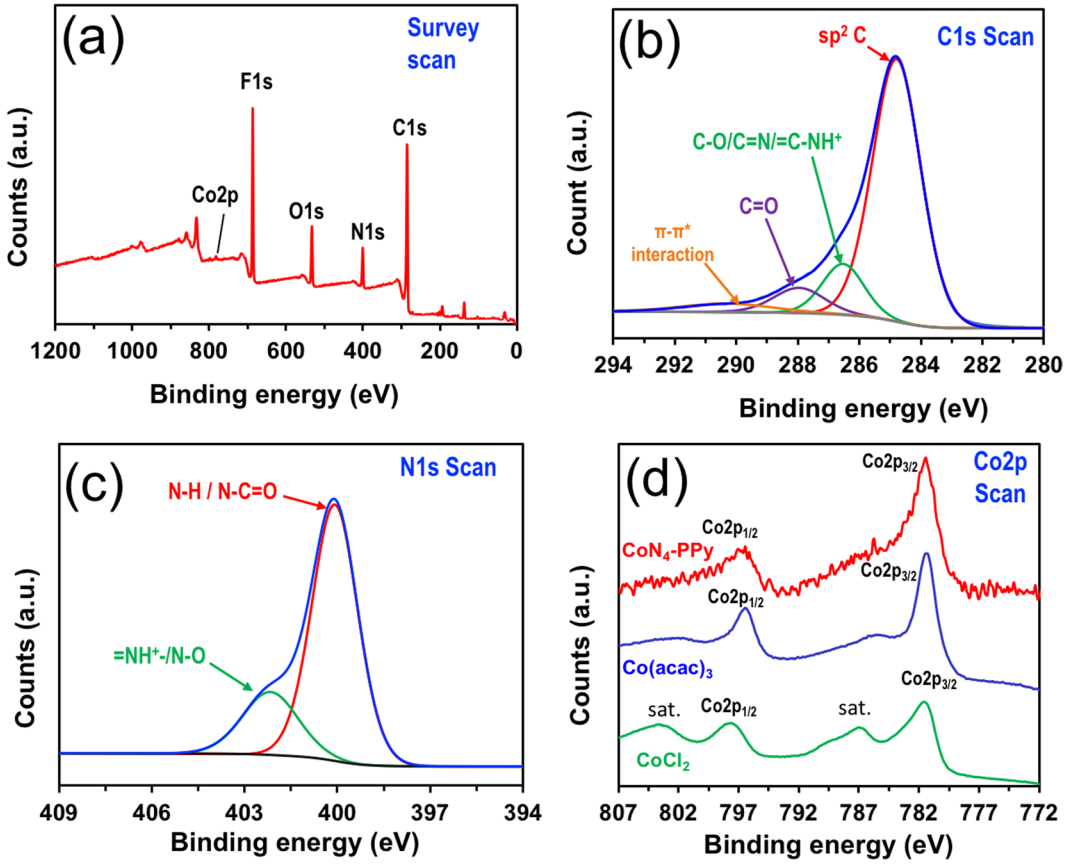


**Figure 2.** (**a**) XPS survey scan of $CoN_4$-PPy film, and a representative XPS narrow scans for (**b**) Carbon (C1s), (**c**) Nitrogen (N1s), and (**d**) Cobalt (Co2p) present in $CoN_4$-PPy film. Figure (**d**) also shows Co2p spectra of $CoCl_2$ and $(Co(acac)_3)$ as reference samples.

## Results and Discussion

**Synthesis and Characterization of $CoN_4$-PPy film.** A scheme for the synthesis of $CoN_4$-PPy film is shown in Fig. 1. Once synthesized, X-ray photoelectron spectroscopy (XPS) was performed to identify the elemental composition, bond formation, and the oxidation state of Co metal in the thin film as shown in Fig. 2.

The survey scan (Fig. 2a) shows the co-existence of C, N, O, and Co, the content of which are provided in Supplementary Table S1. F signal comes from the residual anion of $PF_6^-$ (hexafluorophosphate anion). The narrow scan of C1s spectrum (Fig. 2b) shows several peaks over the range of 284.8 to 289.1 eV. A strong dominant peak at 284.8 eV is assigned to $sp^2$ hybridized carbon present in aromatic ring of PPy[33]. This peak also belongs to carbon atoms present in the aromatic ring and other positions of $CoN_4$ complex. Other carbon peaks at binding energy of 286.5 eV and 287.9 eV indicate the possible formation of C-OH/C=N/=C-$NH^+$ and C=O in the $CoN_4$-PPy film, respectively[33]. The peak positioned at highest binding energy of 290.6 eV can be assigned to π-π* interaction arising from the aromatic rings of PPy or $CoN_4$ complex[33,34]. Nitrogen peak (Fig. 2c) located at 400.1 eV is related to –NH- bond and amide linkage (N-C=O) present in PPy and $CoN_4$ complex, respectively[33,35]. This peak also indicates a contribution from four chemically equivalent nitrogen atoms bound to the metal center (N-Co) in $CoN_4$ complex[36,37]. Further, a peak at higher binding energy value of 402.2 eV is indicative of $=NH^+$-/N-O bonds[33,37]. Similar peaks were seen in the XPS narrow scans of C1s and N1s of PPy film (Supplementary Fig. S1a,b). Further, Co2p narrow scan of $CoN_4$-PPy film revealed two major peaks. The first peak that appeared at 781.8 eV is assigned to $Co2p_{3/2}$ and is most likely Co-$N_x$ bond in $CoN_4$ complex[38]. The second peak at 796.9 eV is ascribed to $Co2p_{1/2}$. The peak separation between these two peaks was approximately 15.1 eV, which is indicative of Co species in +3 oxidation state[39]. To confirm the existence of +3 oxidation state in $CoN_4$-PPy thin film, we performed the XPS of Cobalt(II) chloride ($CoCl_2$) and Cobalt(III)acetylacetonate ($Co(acac)_3$). The shape of Co 2p spectra of these two reference samples were compared with the shape of the Co 2p spectra in $CoN_4$-PPy thin film (Fig. 2d). Similar peak shapes observed in Co2p spectra both for $CoN_4$-PPy and $Co(acac)_3$ indicate that the Co in $CoN_4$-PPy thin film is indeed in +3 oxidation state. Furthermore, two distinct satellite peaks, characteristic for Co in the +2 oxidation state, were displayed in the Co 2p spectra of $CoCl_2$. These satellite peaks were not observed in the $CoN_4$-PPy thin film, which is indicative of Co in the +3 oxidation state in $CoN_4$-PPy thin film.

Further, to monitor any changes in the chemical nature of C, N, and Co after exposure to the highly acidic environment ($HClO_4$) that was used during the supercapacitor performance, XPS of $CoN_4$-PPy film was also conducted. For an acid exposed $CoN_4$-PPy film, the C1s narrow scan indicated slight shifting of the peaks at

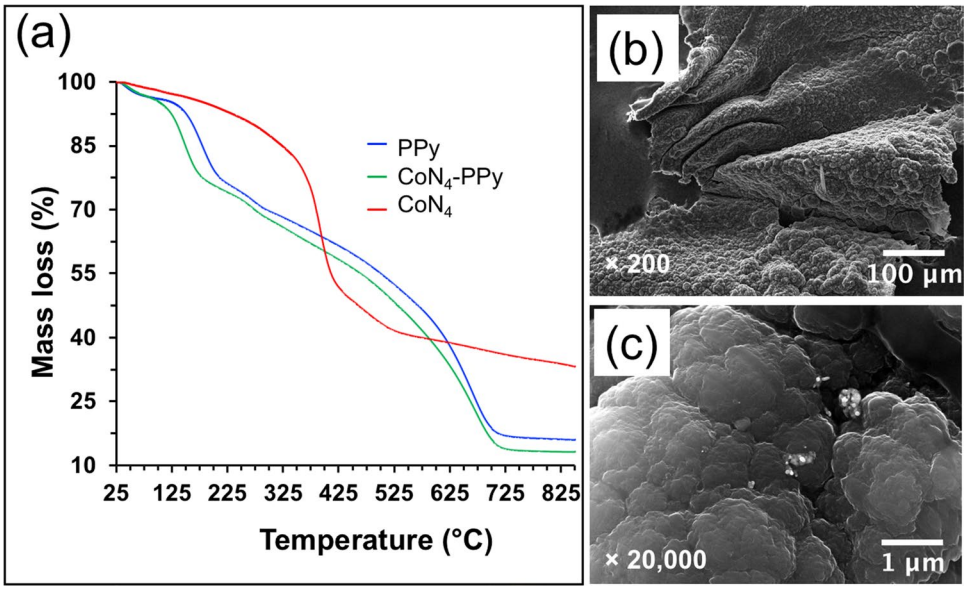


**Figure 3.** (**a**) TGA of PPy, $CoN_4$-PPy and $CoN_4$ thin films. SEM images of $CoN_4$-PPy thin film at (**b**) x200 and (**c**) x20,000 magnifications.

286.5, 287.9, and 290.6 eV to 286.4, 288.6, and 290.3 eV, respectively (Supplementary Fig. S2a). Likewise, the N1s narrow scan show slight shifting of the peaks (Supplementary Fig. S2b). The shifting of these peaks may be due to some mathematical random fluctuation during XPS fitting. Any changes with the Co2p narrow scan would show possible demetallation of Co from the metal complex. Also, shifting in the peak positions, peak separation, and appearance of satellite peaks would indicate any potential changes of the Co metal oxidation in the complex. However, none of these phenomena were observed in the XPS of Co2p narrow scan for the acid exposed $CoN_4$-PPy film. The peak separation between $Co2p_{1/2}$ and $Co2p_{3/2}$ remained to be 15.0 eV indicating Co(III) oxidation state (Supplementary Fig. S2c)[39]. Therefore, it can be inferred from the XPS analysis that the Co metal in $CoN_4$ is stable within the acidic electrolyte which may be attributed to its strong attachment with PPy. This attachment could facilitate the reaction between Co and electrolyte, and thus results in a higher capacitance.

Raman spectroscopy was also used to evaluate the stability of $CoN_4$-PPy films after exposure in acidic solution (Supplementary Fig. S3). The two intense peaks at 1340 and 1570 $cm^{-1}$ correspond with the C-N and C=C stretching frequencies present in PPy, respectively[40]. An additional peak at 1050 $cm^{-1}$ is characteristic of C-H in-plane deformation of PPy[41]. A small range Raman shift was performed to observe the presence of the Co catalyst in the film. A distinct broader peak at 405 $cm^{-1}$ could be attributed to the Co-N stretch[42]. This is slight shift from the 420 $cm^{-1}$ peak observed in a previously synthesized Co(III)-graphene nanocomposite, which could be from the interaction of the Co catalyst with PPy[40]. After exposure to acidic electrolyte, Raman spectroscopy was conducted and revealed no appearance of a band between 3200–3300 $cm^{-1}$, which would indicate N-H stretching frequency present in ligand ($N_4$). Therefore, it can be inferred that the Co(III) complex in $CoN_4$-PPy films is relatively stable in acidic environment even though Co(III) salt is susceptible to dissolve in acidic medium, which may undergo reduction to lower oxidation state such as Co(II). This result was illustrated by our findings with XPS. The perfect morphology of as-synthesized $CoN_4$-PPy thin film, high stability of metal N4 complexes, and greater attachment of metal complex on the PPy surface through $\pi$-$\pi$* interaction and coordination of Co(III) with PPy nitrogen atoms protect the Co(III) complex from getting demetallated in strongly acidic medium. Additionally, Co-complex, which is a square planar complex, provides open coordination sites for PPy nitrogen. Thus, PPy nitrogen easily interacts with the cobalt center holding it tightly in a matrix and stabilize the complex in acidic medium, which would account for the high stability of the thin film, effective ion penetration and/or electron transport and leads to a higher capacitance.

Further characterization of $CoN_4$-PPy was performed using thermogravimetric analysis (TGA) to study the thermal behavior of the thin films (Fig. 3a). The TGA profile of PPy and $CoN_4$-PPy are similar with changes in the onset temperatures of degradation. There are three zones of thermal degradation. The first zone represents the initial loss in mass due to water desorption during heating. The second zone starts around 130 °C for PPy and indicated degradation of the pyrrolic backbone. $CoN_4$-PPy began degradation at 105 °C, which was due to modification of PPy with $CoN_4$. PPy retained more mass loss than $CoN_4$-PPy, which is due to the increased presence of polypyrrole in the sample. It has been shown that higher amounts of PPy retain more mass after thermal degradation compared to materials that have decreased concentration of PPy, and, thus, the reason for greater mass loss in $CoN_4$-PPy.

Surface morphology of $CoN_4$-PPy was conducted using scanning electron microscope (SEM) and images were observed at x200, and x20,000 magnifications (Fig. 3b,c, respectively). The imaging shows uniform film surface with cauliflower-like clusters throughout, which is commonly observed in PPy materials (Fig. 3b)[43]. At higher magnification, the appearance of white clusters becomes noticeable (Fig. 3c). They are attributed to the dispersion

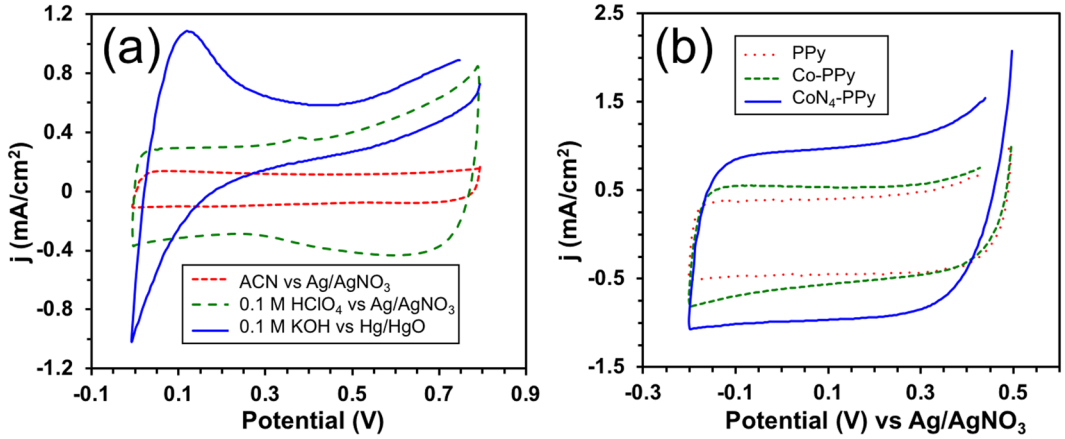


**Figure 4.** (**a**) CVs of PPy films on ACN, 0.1 M $HClO_4$, and 0.1 M KOH electrolyte solutions, scan rate = 5 mV/s and potential scanning = 0 to 0.8 V. (**b**) CVs of PPy, Co-PPy and $CoN_4$-PPy films in 0.1 M $HClO_4$, scan rate = 10 mV/s and potential scanning = −0.2 to 0.5 V (versus $Ag/AgNO_3$).

of $CoN_4$ on PPy film during electrochemical deposition, as is observed in other modified PPy materials[44]. To observe the distribution of Co complex on the surface of $CoN_4$-PPy thin film, energy dispersive X-ray spectroscopy (EDS) elemental mapping on the scanning transmission electron microscopy (STEM) was performed (Supplementary Fig. S4a–e). Fig. S4a is the STEM image of $CoN_4$-PPy thin films and Fig. S4b–e are the corresponding mapping images for C, N, O, and Co elements. The results illustrate uniform distribution of Co complex throughout the surface of the $CoN_4$-PPy thin films despite of its low concentration. The EDS spectra of $CoN_4$-PPy thin film is shown in Fig. S4f, which revealed the presence of C, N, O, and Co. Further, the three-dimensional (3-D) surface morphology, topography, and surface area of the thin film studied with 3-D laser scanning microscopy showed the uniformity of the sample without any cracks and resulted in the total surface area higher by 5.58 times than the initial or the blank surfaces for the scan areas (Supplementary Fig. S5 and Table S2).

**Electrochemical studies (Supercapacitive properties).** *Effect of different electrolytes on supercapacitance.* Cyclic voltammetry (CV) is a powerful tool in the study of capacitive effect of any electrode material where the choice of electrolyte solution plays an equally important role. Thus, to determine the proper electrolyte, CVs of PPy films electrode were conducted using organic and aqueous solvents. Acetonitrile (ACN) was chosen as an organic electrolyte whereas for aqueous electrolytes 0.1 M perchloric acid ($HClO_4$) and 0.1 M potassium hydroxide (KOH) were selected. The result in Fig. 4a displays CVs obtained in different electrolytes when scanned at 5 mV/s in a potential window of 0.0 to 0.8 V. It can be observed that both ACN and 0.1 M $HClO_4$ electrolytes showed great charge and discharge times for PPy films. In ACN, PPy films showed a rectangular type voltammogram with a maximum current density of 750 μA/cm$^2$. The PPy film in ACN was being reduced (discharged) from 0.8 to 0.7 V (versus $Ag/AgNO_3$), as indicated by the rapidly decreasing current, as negatively charged ions in the electrolyte solution left the film causing the film to act as an insulator. The film was fully discharged at this point and remained in its reduced state until the potential was decreased to 0.0 V (versus $Ag/AgNO_3$) at which point the applied scan rate was reversed and began to increase the applied potential.

The PPy film was further being oxidized (charged) from 0.0 to 0.1 V (versus $Ag/AgNO_3$), as indicated by the rapidly increasing current, as negatively charged ions in the electrolyte solution entered the film causing the film to act as a conductor[45]. The PPy film in ACN remained in its oxidized state as the potential increased and reached 0.8 V (versus $Ag/AgNO_3$). A different phenomenon was observed with PPy films in 0.1 M $HClO_4$. Like PPy films in ACN, PPy films in acidic media cycle through both a reduced (discharged) state and an oxidized state (charged). However, unlike PPy films in ACN, PPy films in acidic media never reached a full charge or discharge state; rather, the current started to rapidly increase at about 0.4 V (versus $Ag/AgNO_3$) as the film was being oxidized until it reached a maximum current density at 0.8 V (versus $Ag/AgNO_3$). This was attributed to a set of redox reaction that occured at the films surface indicating that PPy films in acidic media gain charge through both electrostatic forces as well as pseudocapacitative mechanisms[46]. The differences observed in the two media occurred due the nature of the electrolyte solution (aqueous versus organic). In aqueous solvents, their higher ionic conductivity and non-corrosiveness are believed to make them more advantageous than the organic electrolytes[47]. Furthermore, their low cost and lower toxicity benefits their widespread use. When comparing acidic versus alkaline electrolyte, 0.1 M $HClO_4$ was a much better choice for supercapacitor application as seen in Fig. 4a. Redox reactions were observed in the 0.1 M KOH solution at the intense peak at 0.115 V (versus Hg/HgO), which could be due to the redox activity of PPy[48]. The presence of this peak has also been associated with a combination of changes in electronic and ionic conductivity as PPy is transitioning from an insulator to a conductor[48]. From these observations, 0.1 M $HClO_4$ was chosen as the electrolyte solution for additional supercapacitor testing.

*Effect on supercapacitance of different PPy films.* The voltammogram responses of PPy film, PPy film with cobalt acetate (Co-PPy), and $CoN_4$-PPy film were obtained in 0.1 M $HClO_4$ electrolyte at 10 mV/s in a potential range of −0.2 to 0.5 V (versus $Ag/AgNO_3$). The results, depicted in Fig. 4b, indicate that all three samples retained a

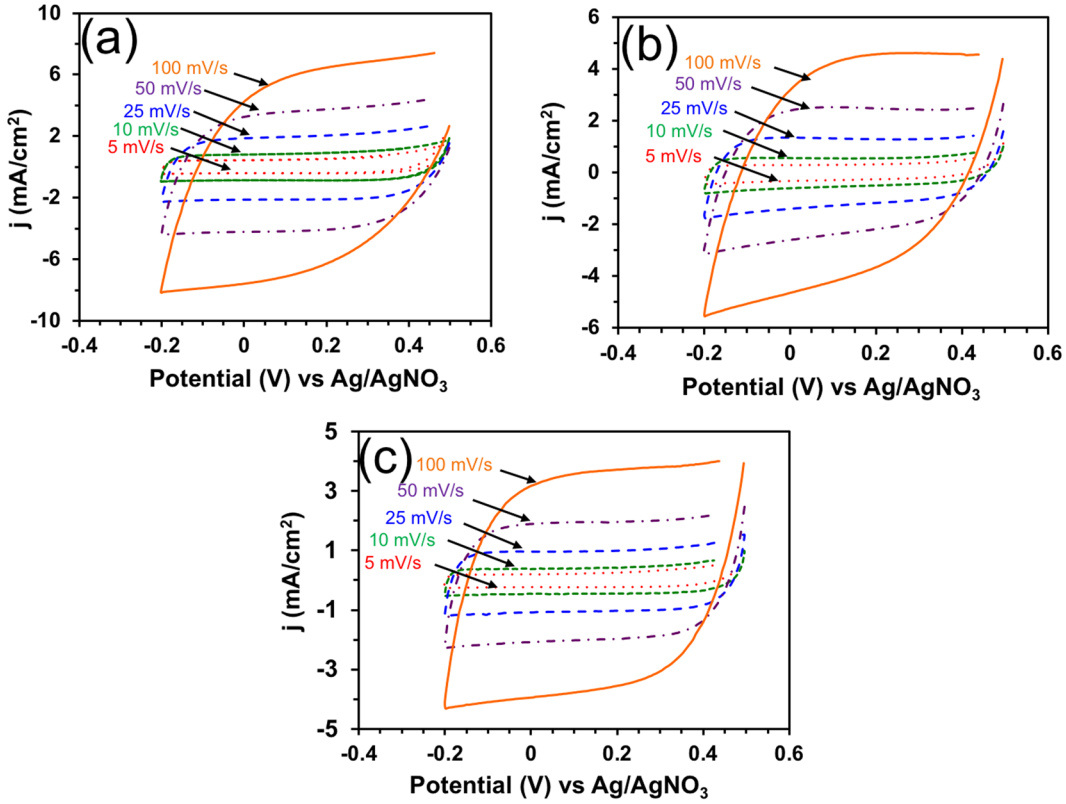


**Figure 5.** CVs of (**a**) $CoN_4$-PPy film (**b**) Co-PPy film and (**c**) PPy film in 0.1 M $HClO_4$ at increasing scan rates from 5 to 100 mV/s. Potential scanning = −0.2 to 0.5 V (versus $Ag/AgNO_3$).

| | *Power (W) ( × $^{10-5}$)* | | | *$i_{avg}$ (mA/cm²) ($^{\times 10-5}$)* | | | *$C_g$ (F/g)* | | |
|---|---|---|---|---|---|---|---|---|---|
| *Scan rate* | PPy film | Co-PPy | $CoN_4$-PPy | PPy film | Co-PPy | $CoN_4$-PPy | PPy film | Co-PPy | $CoN_4$-PPy |
| *5 mV/s* | 4.97 | 8.44 | 1.51 | 6.21 | 1.05 | 2.16 | 216.1 | 351.8 | 721.9 |
| *10 mV/s* | 8.64 | 1.51 | 2.40 | 1.08 | 1.89 | 3.43 | 180.1 | 314.9 | 571.9 |
| *25 mV/s* | 1.87 | 3.32 | 5.10 | 2.34 | 4.15 | 7.29 | 156.0 | 276.6 | 486.4 |
| *50 mV/s* | 3.45 | 6.01 | 8.66 | 4.32 | 7.52 | 1.24 | 144.0 | 250.8 | 412.7 |
| *100 mV/s* | 6.25 | 1.07 | 1.29 | 7.81 | 1.34 | 1.84 | 130.2 | 223.1 | 306.2 |

**Table 1.** Specific capacitance ($C_g$) of PPy, Co-PPy, and $CoN_4$-PPy film at increasing scan rate. Conditions: scan rate from 5 to 100 mV/s, 0.1 M $HClO_4$ electrolyte solution, 25 °C, $Ag/AgNO_3$ reference electrode.

characteristic rectangular type voltammogram suitable for supercapacitance with significant high magnitude of current density. Each film also accumulated charge quickly and dissipated it relatively quickly. $CoN_4$-PPy film exhibited a noticeable increase in current density compared to PPy and Co-PPy films. The current density almost doubled from 0.539 mA/cm² in Co-PPy to 0.979 mA/cm² in $CoN_4$-PPy at 0.110 V (versus $Ag/AgNO_3$).

*Effect of scan rate.* The CVs of PPy films were further performed at increasing scan rates from 5 to 100 mV/s (Fig. 5a-c). It was observed that the scan rate had a profound effect on the amount of current density observed. As the scan rate was increased, the current density also increased for each PPy film in 0.1 M $HClO_4$. Another interesting effect observed was the decreasing rate of charge accumulation and dissipation as the scan rate was increased. This was observed as the shape of the CVs became less rectangular-shaped as the scan rate was increased. From these plots, the $CoN_4$-PPy (Fig. 5a) exhibited the highest current density followed by Co-PPy (Fig. 5b) and PPy (Fig. 5c) films, respectively.

From the CV of each film, the specific capacitance ($C_g$) for each of the three films was calculated by using the relationship between average current density ($i_{avg}$), scan rate ($\nu$) and the mass ($m$) of the films (eq. 1). This equation can further be equated with respect to charge ($Q$) and applied potential ($V$). The $C_g$ of each film was calculated at scan rates from 5 to 100 mV/s and is given in Table 1.

$$C_g = \frac{i_{avg}}{v \cdot m} = \frac{Q}{V \cdot m} \quad (1)$$

A maximum specific capacitance was calculated to be 216.1, 351.8 and 721.9 F/g for PPy, Co-PPy and $CoN_4$-PPy, respectively. The high specific capacitance of $CoN_4$-PPy is greater than that of a Co hydroxide nanowire supported on exfoliated graphite oxide (610 F/g)[20] and Mn and Co oxide nanowire array (480 F/g)[14]. Apart from this, the maximum specific capacitance exhibited by $CoN_4$-PPy at 5 mV/s outstrips the values that were previously reported on PPy based electrode materials (Supplementary Table S3). There are several reasons that can be cited for the increased specific capacitance for the thin films. Co in both cobalt acetate and complex ($CoN_4$) are responsible for providing redox active sites. However, improved solubility of $CoN_4$ compared to Co acetate in 0.1 M $HClO_4$ electrolyte used for electrochemical studies increased the redox active sites in its film. This phenomenon can be explained by the fact that high amount of $CoN_4$ was deposited on PPy film during the electropolymerization process and this contributed to higher current density of $CoN_4$-PPy. As seen in Fig. 4b, the effect of pseudocapacitance was diminished in the $CoN_4$-PPy film compared to Co-PPy at lower potential. The shape of the voltammogram curve for Co-PPy deviated from the characteristic rectangular shape of supercapacitors due to charge-transfer interaction between the electrode surface and the acidic electrolyte[9].

Another possible reason for the increase in the specific capacitance lies in the film preparation. There are two common preparation techniques that were mentioned earlier: chemical precipitation and electrochemical deposition. In the former method, problems of particle agglomeration and presence of a binder hinder the prepared materials[47]. As a result, the active surface area of the material can be decreased, which increases the internal resistance. This generates a lower specific capacitance, as observed in a Co oxide/graphene composite[12]. Electrochemical deposition method that was employed in this study dispersed $CoN_4$ throughout the PPy film, which allows for great active surface area. Consequently, the material generated a high current density with a large specific capacitance.

Finally, unique redox property and the structure of the complex over other Co materials also enhances its ability to hold and maintain charge. Within the complex structure, $CoN_4$ has multiple sites that can undergo reduction/oxidation and, consequently, hold charge. To begin, the Co metal itself acts as a site for charge accumulation. As a transition metal, it has the ability to be easily reduced to a Co(II) state during discharge. The amidomacrocyclic ligand structure also contains areas of potential reduction/oxidation. The four carbonyl groups (C=O) can be reduced during discharge to C-$O^-$ and oxidized back to the carbonyl as the material is being charged. Furthermore, the benzene ring can be reduced. These multiple locations of reduction/oxidation attributed to high charge storage of $CoN_4$-PPy.

We compared our result with some of the recent works that has been done in the supercapacitor fields. In our work, the maximum specific capacitance value obtained using $CoN_4$-PPy film on GCE for supercapacitor in 0.1 M $HClO_4$ was significantly higher for those obtained using GCE modified with (Ag)-PPy/Graphene and mesoporous polyaniline (M-PANI) films in 1 M KOH and 1 M $H_2SO_4$, respectively[18,49]. Further, with respect to other samples that employed PPy but different substrate other than GCE for electrode preparation also lacked higher supercapacitor activity than $CoN_4$-PPy film[8,20,50–53]. It was also found that some electrode materials were fabricated using Pt foil substrate, which use expensive and rare Pt metal[52]. Recently, some groups were successful to achieve specific capacitance value higher than the one we reported in this work. However, in their work reduced graphene oxide (RGO) and metal oxides were used for electrode making in Ni foam substrate[8,13]. Our experiments use Co complex, PPy and GCE substrate to achieve high specific capacitance, which was not reported elsewhere thus far.

The specific capacitance values were plotted with respect to scan rate as given in Fig. 6. The specific capacitance of films decreased quickly with scan rate up to 25 mV/s. At higher scan rates, the specific capacitance did not decrease as quickly, which showed a loss of dependence of the specific capacitance on increasing scan rate. From this plot, it is obvious that $CoN_4$-PPy exhibited a much greater specific capacitance than the other films. Co-PPy had a larger specific capacitance than PPy, which showed how modification of PPy films can enhance its performance. However, the ability of $CoN_4$ to provide more redox active centers for increased charge storage revealed that the nature of Co metal used (Co salt versus a Co catalyst) has a dramatic effect on capacitance.

GCD tests were performed at different current densities for $CoN_4$-PPy in 0.1 M $HClO_4$ electrolyte solution (Supplementary Fig. S7a). Asymmetrical charge and discharge curves were seen, indicating pseudo-capacitance behaviors of the $CoN_4$-PPy thin film[54]. Additionally, the small IR drops, due to the electrode's internal resistances, at the beginning of the discharge processes in the given current densities, were responsible for the non-linear discharge curves. These negligible IR drops can also explain conductivity and improved charge efficiency[54,55]. The specific capacitances values were measured at different current densities from GCD curves using eq. (2).

$$Cs = \frac{It}{\Delta V m} \quad (2)$$

where, $C_s$ is the specific capacitance (F/g), I is the discharge current (A), t represents discharge time (sec), $\Delta V$ is the potential window (V), and m is the mass of the electro active material (g). As calculated from GCD curves using eq. (2), $CoN_4$-PPy displayed the specific capacitances of 668, 564, 467, and 423 F/g at current densities of 0.45, 0.5, 1.5 and 2.5 mA/$cm^2$, respectively. Fig. S7b shows the variation of specific capacitance at different current densities. The results show that the specific capacitance decreases when the applied current density increases. At higher current densities and thus higher polarization, less electrolyte will diffuse into the inner active sites, resulting in decreased specific capacitances[56,57].

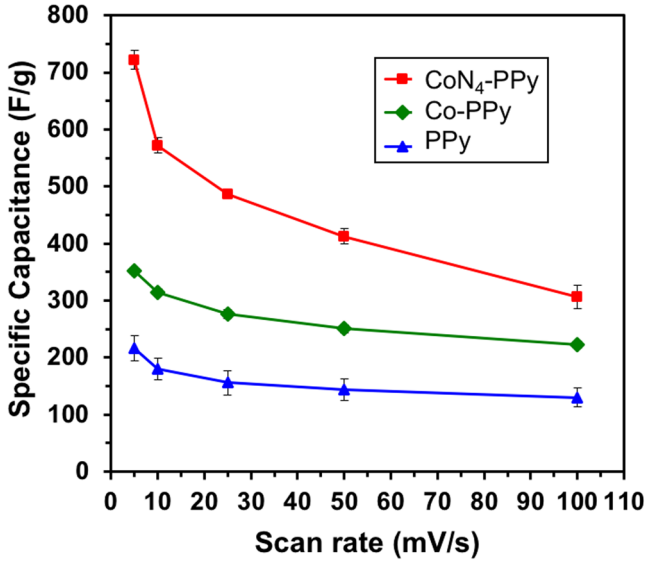


**Figure 6.** Variation of specific capacitance of PPy, Co-PPy and $CoN_4$-PPy films with scan rate in 0.1 M $HClO_4$ electrolyte.

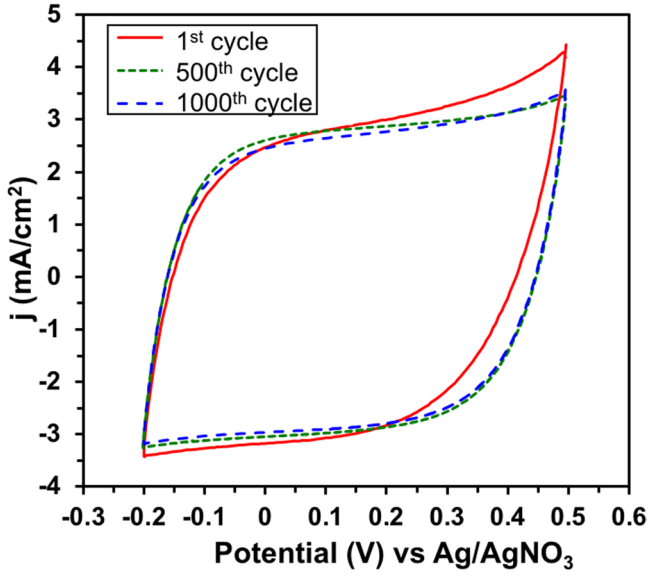


**Figure 7.** Stability of $CoN_4$-PPy film in 0.1 M $HClO_4$, scan rate = 25 mV/s and potential scanning = −0.2 to 0.5 V (versus $Ag/AgNO_3$).

To demonstrate the electrochemical stability of $CoN_4$-PPy, CVs were recorded up to 1000 cycles at 25 mV/s (Fig. 7). From the first cycle to the final, little change in current density was observed. The reason for the change could be due to small pseudocapacitance that is observed in the first cycle but later reduced in the 500$^{th}$ and 1000$^{th}$ cycle. During initial CV, any effect of pseudocapacitance becomes very evident. However, after longer cycles are performed, the degree of pseudocapacitance decreases and the charge storage mechanism shifts from a Faradaic to non-Faradaic process. Overall, $CoN_4$-PPy was found to be electrochemically stable in strongly acidic media. This feature is advantageous for supercapacitors since the electrode material does not need to be replaced often and allows for uses of this material in remote locations[9].

*Effect of electrolyte concentration.* The formation of a double layer within the electrode surface by electrolyte ion mobility depends on the electrolyte concentration[58,59]. Thus, electrolyte concentration has a significant effect on the electrical conductivity and the capacitance of the supercapacitor. Investigating this effect, we chose aqueous hydrochloric acid (HCl) electrolyte because it is one of the most widely used electrolyte solutions for supercapacitor applications. We studied the electrochemical behavior of the $CoN_4$-PPy in 0.01, 0.1 and 1 M HCl by CV at a scan rate of 10 mV/s (Supplementary Fig. S6). As shown in Fig. S6, $CoN_4$-PPy, in 0.1 M and 1 M HCl electrolytes

showed ideal capacitive behavior displaying symmetrical rectangular shape voltammograms with no redox peaks; however, at low concentration (0.01 M), slight distortion of shape was observed which may be due to inadequate conductivity and mobility of ions for building-up the electric double layer. It was also observed that the current density of $CoN_4$-PPy thin film increases gradually with the concentration of HCl electrolyte. In addition, the higher current density observed at higher electrolyte concentration (1 M HCl) indicated greater charge stored by the electrode. This behavior was developed due to high accumulation of electrolyte ion onto the double layer surface and their facile transport within the electrode layer. This observation was consistent with the previous findings[59,60]. Thus, it can be concluded that higher specific capacitance could be possible to achieve when higher electrolyte concentration is used.

*Effect of using different electrochemical cell systems.* Previous findings have established that capacitance value for the supercapacitor electrode material depends strongly on the type of electrochemical cell configurations[61]. In order to investigate this effect, along with three-electrode system, the supercapacitive performance studies of $CoN_4$-PPy thin film, in two-electrode system, were also conducted. CV tests were carried out at a scan rate of 10 mV/s in 0.1 M $HClO_4$ (Supplementary Fig. S8a,b). In can be seen from Fig. S8a that $CoN_4$-PPy, in three-electrode system, showed a rectangular like shape indicating ideal capacitive behavior with reversibility. It also exhibited highest current density which indicated high specific capacitance of the electrode system. However, a different scenario was observed in case of two-electrode system. As shown in Fig. S8b, $CoN_4$-PPy showed a narrower loop but still maintained the characteristic rectangular shape with a slight deviation. The narrower loop indicated low current density and consequently low specific capacitance of the electrode system. Based on the above result, the values of specific capacitance calculated for three- and two-electrode systems were found to be 533 F/g and 175 F/g, respectively. Similar results were most commonly observed for electrochemical supercapacitor materials[61,62]. The extremely high value of specific capacitance found in the case of three-electrode system compared to the two-electrode system illustrates the fact that the latter system only provides a good approximation of electrode performance in supercapacitors[61].

*GCD cyclic stability and electrochemical impedance spectroscopy (EIS) measurement.* The GCD cyclic stability and specific capacitance retention of $CoN_4$-PPy thin film were investigated at applied current density of 0.5 mA/$cm^2$ for 500 cycles in 0.1 M $HClO_4$ (Supplementary Fig. S9a). It was observed that $CoN_4$-PPy retains 93% of the initial capacitance after 500 cycles. Commonly, poor cyclic stabilities were observed with electrically conducting polymer (ECP) films due to the fast degradation of the polymer chains, low electrochemical stabilities, and loss of active materials resulting from the continuous swelling/shrinkage and thus the formation of cracks during cycling[63]. However, past studies have proved that incorporating transition metal ions or complexes or oxides onto the conducting polymers effectively suppress the crack formation of polymeric thin film electrode during cycling and effectively enhanced the electrochemical performance[52,64]. Thus, we believe the inclusion of $CoN_4$ into the PPy film could suppress the cracking of the PPy backbone during GCD cycling and increase its conductivity resulting in the high specific capacitance and improved cyclic stabilities. Additionally, cobalt metallic center in $CoN_4$ can offer more active sites of faradic reaction and facilitate the charge transfer for $CoN_4$-PPy thin film electrode[65,66]. Supplementary Fig. S9a also showed that $CoN_4$-PPy thin film produced fairly stable specific capacitance after 350 cycles, except for the initial 7% decline in specific capacitance. This observed initial decline in specific capacitance may be some of the surface adsorbed $CoN_4$ complex in $CoN_4$-PPy thin film was either leached out or degraded onto the acidic electrolyte solution resulting in decrease of active surface area[67]. The overall improved cyclic stability may be attributed to the affinity of the metal-complex to bind with polypyrrole by $\pi$-$\pi^*$ interaction of benzene rings, counter-ion interactions, and morphology of the sample, which are ideal for easy electrons mobility and charge transfer[66,68]. Further, to study the possible presence of $CoN_4$ or it's degraded form into the electrolyte solution, UV-vis spectroscopic analysis of the electrolyte solution sample withdrawn after 100 cyclic electrochemical measurements in 0.1 M $HClO_4$ was performed (Supplementary Fig. S10). However, the result showed that the concentration of the $CoN_4$ or decomposition product of the sample was not detectable in an appreciable limit into the electrolyte. Electrochemical impedance spectroscopy (EIS) measurements were performed for $CoN_4$-PPy film before and after 500 GCD cycles and the corresponding impedance (real and imaginary) values for both were obtained (Supplementary Fig. S9b). According to the Nyquist plots in Fig. S9b, semi-circles in the high frequency region, which corresponds to a charge-transfer resistances ($R_{ct}$), vary slightly during cycling, further supporting its cycling stability.

## Conclusions

PPy films with $CoN_4$ complex and a cobalt salt ($Co(OAc)_2$) were successfully synthesized by electrochemical oxidation *via* electrochemical deposition. Acidic media proved to be the optimal electrolyte choice over alkaline or organic solvents. The unique redox property and solubility of $CoN_4$ compared to $Co(OAc)_2$, allowed $CoN_4$ to accumulate inside PPy films to a greater extent leading to an increase in overall capacitance. $CoN_4$-PPy had the highest specific capacitance value of 721.9 F/g in 0.1 M $HClO_4$ at a scan rate of 5 mV/s. Moreover, excellent electrochemical stability was observed up to 1000 cycles in acidic media. GCD revealed low rate for charging or discharging, which indicated improved capacitance and charge storage. $CoN_4$-PPy displayed excellent stability and high specific capacitance retention after 500 GCD cycles. The high specific capacitance and ease of synthesis for these films make them ideal electrode materials for supercapacitors.

## Methods

**General.** Chemicals used in this study were purchased from Sigma-Aldrich, USA or Acros Organics, USA and were used as received unless otherwise noted. Pyrrole was distilled using calcium hydride as a drying agent. Nitrogen gas (ultra-high purity) was obtained from NLR Welding Supply Inc. Cyclic voltammetry (CV) studies were performed using a Pine Instrument (Grove City, PA) bipotentiostat (Model AFCBP1) at 25 °C. Galvanostatic charge-discharge (GCD) and electrochemical impedance spectroscopy (EIS) tests were performed using CHI660D electrochemical analyzer. Thermo Scientific K-Alpha X-ray Photoelectron Spectroscopy (XPS) system was utilized to obtain the XPS spectra. Scanning electron microscope (SEM) coupled with energy-dispersive X-ray spectroscopy (EDS) was carried out by using JEOL SEM (JSM 7000 F). Raman spectra were recorded using a Raman spectrometer (Horiba Jobin Yvon LabRam HR800, Edison, New Jersey). Thermogravimetric analysis (TGA) was performed with a Shimadzu DTG-50 thermal analyzer, where samples were heated from 25 to 850 °C at a heating rate of 10 °C/min. Three-dimensional (3D) surface morphology, topography and surface area were evaluated using a laser scanning confocal microscope (LSCM, VK-X260K, Keyence, USA). Samples were scanned using 100X lens and the scanning spot dimension was 108 μm × 145 μm. 3D measurement data collected were analyzed with Keyence's Multi-File Analyzer software. UV-vis spectroscopy was performed using AGILENT (Varian) Cary 5000 Spectrophotometer, USA.

**Synthesis of ligand ($N_4$) and Co(III) complex ($CoN_4$).** Synthesis of the amidomacrocyclic ligand ($N_4$) was conducted following a previously published procedure[69] using 4,5-dichloro-*o*-phenylene diamine to generate the dichloro version of this ligand. Synthesis of the cobalt complex was performed as follows. In a 100-mL Schlenk flask containing a magnetic stir bar, $N_4$ (200 mg, 0.45 mmol) was added and dissolved in 20 mL dry tetrahydrofuran (THF) by stirring under $N_2$ atmosphere at 25 °C. After dissolution, the temperature was lowered to 0 °C by placing the flask in an ice bath. Once the solution was cooled, *n*-butyllithium (0.74 mL, 1.8 mmol, 2.5 M in hexanes) was added, followed by anhydrous cobalt (II) chloride (64 mg, 0.50 mmol). The reaction was slowly warmed to room temperature and allowed to stir overnight under $N_2$ atmosphere. The reaction yielded a precipitate, which was exposed to air to allow the cobalt to oxidize from Co(II) to Co(III). The THF was removed under vacuum and the solid purple product (Co(III) complex) obtained was further dried under vacuum for 6 h. Yield: 78% (175 mg). The Co(III) complex was converted to the water insoluble form by addition of tetraphenylphosphonium chloride to generate $CoN_4$[70].

**Electrochemical deposition of films.** The synthetic approach for the electrochemical synthesis of PPy thin films was reported earlier[71]. For the synthesis of PPy films, 20 mM of distilled pyrrole dried over calcium hydride was used. 10 mL solutions containing a 1:1 volumetric ratio of propylene carbonate and acetonitrile (ACN) and 50 mM of tetrabutylammonium hexafluorophosphate ($TBAPF_6$) as the supporting electrolyte was prepared as the solution from which deposition was performed. The potential was scanned from 0.00 to 1.20 V at a scan rate of 100 mV/s for 25 cycles, which allowed ten minutes for deposition. After deposition, the film was washed with distilled water followed by an ACN wash and allowed to dry. In a similar manner, $CoN_4$-PPy films were synthesized using 20 mM of pyrrole and 20 mM of $CoN_4$ catalyst. A last set of films called Co-PPy films were deposited using 20 mM of pyrrole and 10 mM of cobalt acetate ($Co(OAc)_2$). Following electrochemical deposition, the three films-PPy, $CoN_4$-PPy and Co-PPy were tested for supercapacitance. All electrochemical synthesis used a three-electrode electrochemical cell. The working electrode was a glassy carbon electrode (GCE), the reference electrode was $Ag/AgNO_3$ ($AgNO_3$ in ACN) and the counter electrode was a platinum (Pt) wire.

**Electrochemical studies.** CV was performed with a potential range from 0.8 to 0 V at varying scan rate of 5 to 100 mV/s, unless otherwise noted. GCD tests were performed within a potential range from −0.2 to 0.4 V at different current densities (0.45, 0.5, 1.5 and 2.5 $mA/cm^2$). EIS measurements were obtained at an amplitude voltage of 5 mV from 1 Hz to 1 MHz in 0.1 M $HClO_4$. A three-electrode system using a GCE working electrode, $Ag/AgNO_3$ reference electrode in acidic media and Hg/HgO in basic media and platinum counter electrode was used when performing CV, GCD, and EIS. In case of two-electrode system in acidic condition, electrochemical cell consists of GCE as working electrode and Pt wire as both reference and counter electrode. All electrochemical tests were performed at room temperature. Within the electrochemical cell, the electrolyte was purged with $N_2$ for at least 30 min prior to use. Voltammograms presented show the average of three trials.

**X-ray Photoelectron spectroscopy.** XPS analysis was carried out with a Thermo Scientific Model K-Alpha XPS instrument using monochromatic Al Kα radiation (1486.7 eV) with the X-ray spot size 200 μm for each sample. The base pressure in the analysis chamber was typically $1 \times 10^{-9}$ mbar. Samples were mounted to the sample platten using double-sided tape. All spectra were collected with the charge neutralization flood gun turned on. The typical pressure during the analysis with the flood gun on was $2 \times 10^{-7}$ mbar. The collected data were processed using the Thermo Scientific Advantage XPS software package. Spectral charge correction was performed using the main C 1 s peak due to hydrocarbon (C-C/C-H bonds) set to 284.8 eV. Mixed Gaussian-Lorentzian peak shapes and a Shirley/Smart type background subtraction were utilized in the peak analysis/fitting.

**Raman spectroscopy.** Raman spectra were recorded using a Raman spectrometer (Horiba Jobin Yvon LabRam HR800, Edison, New Jersey) occupied by He-Ne laser (17 mW) with wavelength of 784 nm and three Olympus BX-51 lenses with 100x micro objectives magnitude connected to a Peltier-cooled CCD camera. The spectra were collected using 600-line/mm grating with the same acquisition time. In all measurements, the Raman spectrometer was calibrated using the Si-Si Raman signal, which is located at a 521 $cm^{-1}$ Raman shift, and conducted at room temperature.

## References


1. Pimentel, D. *et al*. Renewable energy: Current and potential issues renewable energy technologies could, if developed and implemented, provide nearly 50% of US energy needs; this would require about 17% of US land resources. *Bioscience* **52**, 1111–1120 (2002).
2. Sahoo, R., Pal, A. & Pal, T. 2D materials for renewable energy storage devices: outlook and challenges. *Chem. Commun.* **52**, 13528–13542 (2016).
3. Wang, J. *et al*. Smart network node based on hybrid nanogenerator for self-powered multifunctional sensing. *Nano Energy* **33**, 418–426 (2017).
4. Liu, C., Li, F., Ma, L. P. & Cheng, H.-M. Advanced materials for energy storage. *Adv. Mater.* **22**, E28–E62 (2010).
5. Miller, J. R., Simon, P. & Patrice, S. Electrochemical capacitors for energy management. *Science.* **321**, 651–652 (2008).
6. Vlad, A. *et al*. Hybrid supercapacitor-battery materials for fast electrochemical charge storage. *Sci. Rep.* **4**, 4315 (2015).
7. Simon, P., Gogotsi, Y. & Dunn, B. Where do batteries end and supercapacitors begin? *Science.* **343**, 1210–1211 (2014).
8. Asen, P. & Shahrokhian, S. A high performance supercapacitor based on graphene/polypyrrole/$Cu_2O$–$Cu(OH)_2$ ternary nanocomposite coated on nickel foam. *The J. Phys. Chem. C* **121** (2017).
9. Iro, Z. S., Subramani, C. & Dash, S. S. A brief review on electrode materials for supercapacitor. *Int. J. of Electrochem. Sci.* **11**, 10628–10643 (2016).
10. Rajagopalan, B. & Chung, J. Reduced chemically modified graphene oxide for supercapacitor electrode. *Nanoscale Res. Lett.* **9**, 535 (2014).
11. Liu, X. *et al*. Hollow, spherical nitrogen-rich porous carbon shells obtained from a porous organic framework for the supercapacitor. *ACS Appl. Mater. Interfaces* **5**, 10280–10287 (2013).
12. Lei, Y. *et al*. Rapid microwave-assisted green synthesis of 3D hierarchical flower-shaped NiCo2O4 microsphere for high-performance supercapacitor. *ACS Appl. Mater. Interfaces* **6**, 1773–1780 (2014).
13. Pathak, A., Gangan, A. S., Ratha, S. & Chakraborty, B. Enhanced pseudocapacitance of $MoO_3$-reduced graphene oxide hybrids with insight from density functional theory investigations. *J. Phys. Chem. C* **121**, 18992–19001 (2017).
14. Liu, J. *et al*. $Co_3O_4$ nanowire @$MnO_2$ ultrathin nanosheet core/shell arrays: a new class of high-performance pseudocapacitive materials. *Adv. Mater.* **23**, 2076–2081 (2011).
15. Ali, G. A. M., Fouad, O. A., Makhlouf, S. A., Yusoff, M. M. & Chong, K. F. $Co_3O_4/SiO_2$ nanocomposites for supercapacitor application. *J. Solid State Electrochem.* **18**, 2505–2512 (2014).
16. Yan, M. *et al*. Construction of a hierarchical $NiCo_2S_4$@PPy core–shell heterostructure nanotube array on Ni foam for a high-performance asymmetric supercapacitor. *ACS Appl. Mater. Interfaces* **8**, 24525–24535 (2016).
17. Shen, L. *et al*. $NiCo_2S_4$ Nanosheets Grown on Nitrogen-Doped Carbon Foams as an Advanced Electrode for Supercapacitors. *Adv. Energy Mater.* **5**, 1400977 (2015).
18. Khdary, N. H., Abdesalam, M. E. & Enany, G. El Mesoporous polyaniline films for high performance supercapacitors. *J. Electrochem. Soc.* **161**, 63–68 (2014).
19. Patil, B. H., Jagadale, A. D. & Lokhande, C. D. Synthesis of polythiophene thin films by simple successive ionic layer adsorption and reaction (SILAR) method for supercapacitor application. *Synth. Met.* **162**, 1400–1405 (2012).
20. Cai, X. *et al*. High-performance asymmetric pseudocapacitor cell based on cobalt hydroxide/graphene and polypyrrole/graphene electrodes. *J. Power Sources* **275**, 298–304 (2015).
21. Simon, P. & Gogotsi, Y. Materials for electrochemical capacitors. *Nat. Mater.* **7**, 845–854 (2008).
22. Wang, G., Zhang, L. & Zhang, J. A review of electrode materials for electrochemical supercapacitors. *Chem. Soc. Rev.* **41**, 797–828 (2012).
23. Bora, C., Sharma, J. & Dolui, S. Polypyrrole/sulfonated graphene composite as electrode material for supercapacitor. *J. Phys. Chem. C* **118**, 29688–29694 (2014).
24. Huang, S. *et al*. Electrodeposition of polypyrrole on carbon nanotube-coated cotton fabrics for all-solid flexible supercapacitor electrodes. *RSC Adv.* **6**, 13359–13364 (2016).
25. Brushett, F. R. *et al*. A carbon-supported copper complex of 3,5-diamino-1,2,4-triazole as a Cathode Catalyst for alkaline fuel cell applications. *J. Am. Chem. Soc.* **132**, 12185–12187 (2010).
26. Elzing, A., Van Der Putten, A., Visscher, W. & Barendrecht, E. The cathodic reduction of oxygen at cobalt phthalocyanine. *Influence of electrode preparation on electrocatalysis. J. Electroanal. Chem.* **200**, 313–322 (1986).
27. Richards, G. & Swavey, S. Electrooxidation of Fe, Co, Ni and Cu metalloporphyrins on edge-plane pyrolytic graphite electrodes and their electrocatalytic ability towards the reduction of molecular oxygen in acidic media. *Eur. J. Inorg. Chem.* **2009**, 5367–5376 (2009).
28. Gartia, Y. *et al*. Graphene-enhanced oxygen reduction by $MN_4$ type cobalt(III) catalyst. *ACS Sustain. Chem. Eng.* **3**, 97–102 (2015).
29. Nasini, U. B. *et al*. Oxygen reduction reaction catalyzed by cobalt(III) complexes of macrocyclic ligands supported on multiwalled carbon nanotubes. *Chem. Phys. Lett.* **566**, 38–43 (2013).
30. Matsuda, S., Mori, S., Hashimoto, K. & Nakanishi, S. Transition metal complexes with macrocyclic ligands serve as efficient electrocatalysts for aprotic oxygen evolution on $Li_2O_2$. *J. Phys. Chem. C* **118**, 28435–28439 (2014).
31. Wayland, H. A. *et al*. Graphene-supported cobalt(III) complex of a tetraamidomacrocyclic ligand for oxygen reduction reaction. *Catal. Letters* **148**, 407–417 (123AD).
32. Parnell, C. M. *et al*. Polydopamine-coated manganese complex/graphene nanocomposite for enhanced electrocatalytic activity towards oxygen reduction. *Sci. Rep.* **6**, 31415 (2016).
33. Ruangchuay, L., Schwank, J. & Sirivat, A. Surface degradation of α-naphthalene sulfonate-doped polypyrrole during XPS characterization. *Appl. Surf. Sci.* **199**, 128–137 (2002).
34. Su, N., Li, H. B., Yuan, S. J., Yi, S. P. & Yin, E. Q. Synthesis and characterization of polypyrrole doped with anionic spherical polyelectrolyte brushes. *Express Polym. Lett.* **6**, 697–705 (2012).
35. Artyushkova, K., Pylypenko, S., Olson, T. S., Fulghum, J. E. & Atanassov, P. Predictive modeling of electrocatalyst structure based on structure-to-property correlations of X-ray photoelectron spectroscopic and electrochemical measurements. *Langmuir* **24**, 9082–9088 (2008).
36. Koslowski, U. *et al*. Evaluation and Analysis of PEMFC performance using non-platinum cathode catalysts based on pyrolysed Fe- and Co-porphyrins - Influence of a secondary heat-treatment. in *ECS Transactions* **13**, 125–141 (ECS, 2008).
37. Müller, K. *et al*. Spectroscopic characterization of cobalt–Phthalocyanine electrocatalysts for fuel cell applications. *Solid State Ionics* **216**, 78–82 (2012).
38. Samireddi, S. *et al*. Hybrid bimetallic-N4 electrocatalyst derived from a pyrolyzed ferrocene–Co-corrole complex for oxygen reduction reaction. *J. Mater. Chem. A* **5**, 9279–9286 (2017).
39. Biesinger, M. C. *et al*. Resolving surface chemical states in XPS analysis of first row transition metals, oxides and hydroxides: Cr, Mn, Fe, Co and Ni. *Appl. Surf. Sci.* **257**, 2717–2730 (2011).
40. Feng, W. *et al*. A comparative study of pyrolyzed and doped cobalt-polypyrrole eletrocatalysts for oxygen reduction reaction. *Appl. Surf. Sci.* **258**, 4048–4053 (2012).
41. Liu, Y. C. & Hwang, B. J. Identification of oxidized polypyrrole on Raman spectrum. *Synth. Met.* **113**, 203–207 (2000).
42. Nakamoto, K. *Infrared and Raman spectra of inorganic and coordination compounds* (Wiley-Blackwell, 2008).
43. Brisolari, A. & Gonçalves, D. Immobilization of tyrosinase from avocado crude extract in polypyrrole films for inhibitive detection of benzoic acid. *Chemosensors* **2**, 182–192 (2014).

44. Zhang, T., Yuan, R., Chai, Y., Li, W. & Ling, S. A novel nonenzymatic hydrogen peroxide sensor based on a polypyrrole nanowire-copper nanocomposite modified gold electrode. *Sensors* **8**, 5141–5152 (2008).
45. Ansari, R. Polypyrrole conducting electroactive polymers: synthesis and stability studies. *E-journal Chem.* **3**, 186–201 (2006).
46. Bard, A. J. & Faulkner, L. R. *Electrochemical methods: fundamentals and applications* (Wiley, 2001).
47. Zhao, C. & Zheng, W. A review for aqueous electrochemical supercapacitors. *Front. Energy Res.* **3**, 1–11 (2015).
48. Peng, C., Jin, J. & Chen, G. Z. A comparative study on electrochemical co-deposition and capacitance of composite films of conducting polymers and carbon nanotubes. *Electrochim. Acta* **53**, 525–537 (2007).
49. Dhibar, S. & Das, C. K. Silver nanoparticles decorated polypyrrole/graphene nanocomposite: A potential candidate for next-generation supercapacitor electrode material. *J. Appl. Polym. Sci.* **134**, 1–14 (2017).
50. Dubal, D. P., Lee, S. H., Kim, J. G., Kim, W. B. & Lokhande, C. D. Porous polypyrrole clusters prepared by electropolymerization for a high performance supercapacitor. *J. Mater. Chem.* **22**, 3044 (2012).
51. Wu, G. *et al*. High-performance supercapacitors based on electrochemical-induced vertical-aligned carbon nanotubes and polyaniline nanocomposite electrodes. *Sci. Rep.* **7**, 1–8 (2017).
52. Eeu, Y. C., Lim, H. N., Lim, Y. S., Zakarya, S. A. & Huang, N. M. Electrodeposition of polypyrrole/reduced graphene oxide/iron oxide nanocomposite as supercapacitor electrode material. *J. Nanomater.* **2013**, 1–6 (2013).
53. Liu, A., Li, C., Bai, H. & Shi, G. Electrochemical deposition of polypyrrole/sulfonated graphene composite films. *J. Phys. Chem. C* **114**, 22783–22789 (2010).
54. Abdul Bashid, H. A. *et al*. Electrodeposition of polypyrrole and reduced graphene oxide onto carbon bundle fibre as electrode for supercapacitor. *Nanoscale Res. Lett.* **12**, 246 (2017).
55. Chen, J. *et al*. Facile co-electrodeposition method for high-performance supercapacitor based on reduced graphene oxide/polypyrrole composite film. *ACS Appl. Mater. Interfaces* **9**, 19831–19842 (2017).
56. Asen, P. & Shahrokhian, S. A high performance supercapacitor based on graphene/polypyrrole/$Cu_2O$–$Cu(OH)_2$ ternary nanocomposite coated on nickel foam. *J. Phys. Chem. C* **121**, 6508–6519 (2017).
57. Zou, Y. & Wang, S. Interconnecting carbon fibers with the *in-situ* electrochemically exfoliated graphene as advanced binder-free electrode materials for flexible supercapacitor. *Sci. Rep.* **5**, 1–7 (2015).
58. Zheng, J. P. & Jow, T. R. The effect of salt concentration in electrolytes on the maximum energy storage for double layer capacitors. *J. Electrochem. Soc.* **144**, 2417 (1997).
59. Tsay, K.-C., Zhang, L. & Zhang, J. Effects of electrode layer composition/thickness and electrolyte concentration on both specific capacitance and energy density of supercapacitor. *Electrochim. Acta* **60**, 428–436 (2012).
60. Weng, T.-W., Huang, W. & Lee, K.-Y. Improved electrochemical capacitive characteristics by controlling the carbon nanotube morphology and electrolyte solution concentration. *Vacuum* **83**, 629–632 (2008).
61. Khomenko, V., Frackowiak, E. & Béguin, F. Determination of the specific capacitance of conducting polymer/nanotubes composite electrodes using different cell configurations. *Electrochim. Acta* **50**, 2499–2506 (2005).
62. Koysuren, O., Du, C., Pan, N. & Bayram, G. Preparation and comparison of two electrodes for supercapacitors: Pani/CNT/Ni and Pani/Alizarin-treated nickel. *J. Appl. Polym. Sci.* **113**, 1070–1081 (2009).
63. Frackowiak, E., Khomenko, V., Jurewicz, K., Lota, K. & Béguin, F. Supercapacitors based on conducting polymers/nanotubes composites. *J. Power Sources* **153**, 413–418 (2006).
64. Chen, Y., Li, J., Zhang, X. & Xu, H. Effects of transition metal ions on the electrochemical performance of polypyrrole electrode. *J. Mater. Sci. Mater. Electron.* **29**, 11020–11029 (2018).
65. Chen, Y., Kang, G., Xu, H. & Kang, L. PPy doped with different metal sulphate as electrode materials for supercapacitors. *Russ. J. Electrochem.* **53**, 359–365 (2017).
66. Bidan, G., Divisia-Blohorn, B., Lapkowski, M., Kern, J. M. & Sauvage, J. P. Electroactive films of polypyrroles containing complexing cavities preformed by entwining ligands on metallic centers. *J. Am. Chem. Soc.* **114**, 5986–5994 (1992).
67. Soudan, P., Gaudet, J., Guay, D., Bélanger, D. & Schulz, R. Electrochemical properties of ruthenium-based nanocrystalline materials as electrodes for supercapacitors. *Chem. Mater.* **14**, 1210–1215 (2002).
68. Zhang, H., Zhang, Y., Gu, C. & Ma, Y. Electropolymerized conjugated microporous poly(zinc-porphyrin) films as potential electrode materials in supercapacitors. *Adv. Energy Mater.* **5**, 1402175 (2015).
69. Ramidi, P. *et al*. Catalytic cyclic carbonate synthesis using epoxide and carbon dioxide: Combined catalytic effect of both cation and anion of an ionic CrV(O) amido macrocyclic complex. *Ind. Eng. Chem. Res.* **50**, 7800–7807 (2011).
70. Ghosh, A. *et al*. Cycloaddition of $CO_2$ to epoxides using a highly active Co(III) complex of tetraamidomacrocyclic ligand. *Catal. Letters* **137**, 1–7 (2010).
71. Joo, J. *et al*. Physical characterization of electrochemically and chemically synthesized polypyrroles. *Macromolecules* **33**, 5131–5136 (2000).


## Acknowledgements

Funding for this research was provided by the Center for Advanced Surface Engineering, under the National Science Foundation Grant No. IIA-1457888 and the Arkansas EPSCoR Program, ASSET III.

## Author Contributions

C.M.P., B.P.C., T.B.M., F.W., A.B.R., H.Z., K.M.A., G.K. and A.S.B. contributed to the experimental and data interpretation. A.G. conceived the study and experimental design. C.M.P., A.G. and B.P.C. contributed to the experimental design and wrote the manuscript. C.M.P., T.B.M. and B.P.C. contributed to catalyst synthesis. All authors reviewed and approved of the final version of the manuscript.

## Additional Information

**Supplementary information** accompanies this paper at https://doi.org/10.1038/s41598-019-41969-6.

**Competing Interests:** The authors declare no competing interests.

**Publisher's note:** Springer Nature remains neutral with regard to jurisdictional claims in published maps and institutional affiliations.